

Synthesis of $\text{Cu}_2\text{CoSnS}_4$ chalcogenide thin films by spray pyrolysis and efficient Au/p-CCTS/ n- SnO_2 diode for cells solar applications

F. Harrathi^{1,2}, N. Bitri¹, E. Aubry^{3,4}, P. Briois³

1 Laboratoire de Photovoltaïque et matériaux semi-conducteurs, Ecole Nationale d'Ingénieurs de Tunis, Université de Tunis El Manar, Tunis 1002, Tunisie

2 Ecole Nationale Supérieure d'Ingénieurs de Tunis, Université de Tunis, 5 Avenue Taha Hussein, Tunis 1008, Tunisie

3 Institut FEMTO-ST, UMR 6174, CNRS, UTBM, Site de Montbéliard, 90010 Belfort, France

4 Institut FEMTO-ST, UMR 6174, CNRS, UFC, 2 Place Lucien Tharradin, Site de Montbéliard, 25200 Montbéliard, France

* Corresponding author : harrathifaouzia077@gmail.com

Abstract :

Quaternary chalcogenide $\text{Cu}_2\text{CoSnS}_4$ (CCTS) thin films were successfully prepared by spray pyrolysis on glass substrates in varying the precursor concentration and the thiourea volume. The effects of the precursor concentration and the thiourea volume on the formation of the CCTS phase were systematically investigated by X-ray diffraction (XRD), Raman spectroscopy, Energy-Dispersive X-ray Spectroscopy (EDS). The electrical resistivity at room temperature has been measured by the four probes method. It is shown that the crystallization of the stannite CCTS phase depends on both the precursor concentration and thiourea volume. The minimum volume of thiourea required to crystallize the CCTS phase depends on the precursor concentration, i.e. the CCTS crystallization needs higher volume of thiourea at low precursor concentration. For higher precursor concentration, the CCTS is poorly crystallized with the presence of secondary phases such as CuS_2 , CoS_2 , and CuCo_2S_4 , while the crystallization domain is relatively large. The CCTS well crystallizes only in a narrow range of precursor concentration and thiourea volume. The relatively poor crystallization combined with the presence of secondary phases are harmful for the optical and electrical features of the CCTS film. Besides, optical transmission measurements of the optimized film showed an optical gap of 1.7 eV (~ 730 nm) and an absorption coefficient included between 10^4 - 10^5 cm^{-1} in the visible solar range. Furthermore, the optimized stannite CCTS films are compact exhibiting a relatively rough and granular surface due to the formation of copper sulfide nodules. The electrical resistivity of the optimized CCTS film is about $0.4 \cdot 10^{-2}$ $\Omega\cdot\text{cm}$. These results suggest that the deposited films fit the requirements of absorbing layer in solar cells. The diode composed of Au/ $\text{Cu}_2\text{CoSnS}_4$ / SnO_2 films was investigated with current-voltage (I-

V) measurements performed under dark and bright conditions. Ideality factor, series resistance and saturation current of typical diode is estimated to be 3, 689 Ω and $5 \cdot 10^{-6}$ A, respectively.

Keywords: $\text{Cu}_2\text{CoSnS}_4$; thin films; chemical synthesis; thiourea concentration; precursor concentration; spray pyrolysis; solar cells.

1. Introduction

Contrary to fossil fuels, which are distributed in limited areas on Earth and emit toxic CO_2 gas, the sun is a free and unlimited source of energy that is globally distributed. This type of energy allows us to reduce our dependence on fossil fuels. To harness it, multiple electrical contacts, also called solar cells or photovoltaic cells are used. Its purpose is to convert white light into electricity. The current research in the field of solar cells is focused on a new generation which uses thin films and is not based on silicon anymore. In contrast, thin-film photovoltaic technologies rely on direct band gap materials with thicknesses of 1-2 μm being sufficient to absorb most of the incident light. As absorbent layers, cadmium telluride CdTe and copper indium gallium selenide CIGS thin films are efficient, but their toxicity and the rarefy of some elements composing them make crucial the definition of other materials. To overcome this problem, recent research has focused on absorbers composed of earth-abundant elements, cheap to extract and transform, and non-toxic [1]. The quaternary copper-cobalt-tin-sulfide compound $\text{Cu}_2\text{CoSnS}_4$ (CCTS) is one of the promising candidates because it is non-toxic and abundant in the earth's crust [2], [3]. Also, the materials exhibit intrinsic p-type conductivity, an optical energy band gap of around 1.5 eV [4], and an absorption coefficient greater than 10^4 cm^{-1} [5] [6] [7]. CCTS thin films also have other potential applications such as thermoelectricity [8] [9], photocatalysis of water for hydrogen production [10], and electro-catalysis [11]. CCTS films are obtained by various film deposition techniques such as electrospinning [12], injection [10], solid-state reaction [13], solvothermal [11], and spray [4], [14]–[16]. The spray pyrolysis process is a widely used elaboration technique due to its advantages such as easy control of deposition conditions, simplicity, ability to treat large areas at low cost, and environmental friendliness [17]. Despite the simplicity of the technique, the formation of the stannite-structured CCTS film requires a better comprehension regarding the influence of the numerous involved parameters (solution parameters, spray parameters and

crystallization parameters) [18]. The influence of the substrate temperature on the CCTS thin film is probably one of the most studied parameters [7]. The respective concentration of each constituent affects obviously the stoichiometry of the films. However, the precursor solution composed with the appropriate concentration of the constituents affects the nucleation and growth of thin films, which in turn affects the crystallinity, morphology, and composition of the films. In addition, the precursor solution can impact the deposition rate of the thin film and thus the thickness and uniformity of the film [18] [19] [20]. [4]. In addition, the thiourea volume is less study despite it is considered one of the most important process variables which would also act on the stoichiometry of the thin film and on its features. The original purpose of this project was to bring a deeper understanding of the precursor solution and thiourea volume on the growth of CCTS stannite thin films and its resulting properties. The CCTS materials were first dissolved in a solvent with different precursor concentrations and thiourea volumes. The synthesized nanoparticles are dispersed in an environmentally friendly solvent (distilled water) to fabricate a thin film. Using an aqueous solution ensures the uniformity of the thin film with better structural, optical and electrical properties, which makes it more suitable as an absorber layer in thin film solar cells [16] [21] [22] [23]. More importantly, optical and electrical characterizations on CCTS were systematically performed in order to understand process parameters such as precursor concentration and thiourea volume. Finally, the CCTS stannite films was introduced in diode composed of Au/Cu₂CoSnS₄/SnO₂ films and the current-voltage I-V was investigated under dark and light conditions.

2. Experimental details

2.1. Synthesis of CCTS thin films

The precursor solution was obtained by mixing copper chloride (10 mL of CuCl₂·2H₂O), cobalt chloride (5 mL of CoCl₂·6H₂O), tin chloride (5 mL of SnCl₂·2H₂O) and thiourea (SC(NH₂)₂) solutions. The precursor solution was dissolved in distilled water in adjusting the concentration from 0.08 to 0.11 M with an interval of 0.01 M. Then, the solutions were mixed in a beaker under magnetic stirring for a few seconds to maintain transparency and homogeneity. In the first series of experiments, only 70 ml of thiourea was used (CCTS-1 samples). In the second and third set of experiments (CCTS-2 and CCTS-3 samples, respectively), 80 and 90 mL of thiourea was mixed

to the spray solution. The glass substrates were cleaned with a detergent, washed with 3% nitric acid, rinsed with water and acetone, then dried in an oven at 120 °C for 15 min. The spray solution rate was fixed at 3 ml min⁻¹ and the reaction time has lasted for 30 min. The compressed air was used as a carrier gas. The distance between the substrate and nozzle was fixed at 20 cm and the hot plate rotation speed was set at 14 rpm. The plate temperature was fixed at 320 °C under atmospheric conditions. After deposition, the final samples were naturally cooled down at room temperature.

Table 1 Volumes of the precursor solutions mixed for the spray solution. The concentration of the precursor solution varied from 0.08 to 0.11 M with an interval of 0.01 M.

	Copper chloride (CuCl ₂ .2H ₂ O) mL	Cobalt chloride (CoCl ₂ .6H ₂ O) mL	Tin chloride (SnCl ₂ .2H ₂ O) mL	Thiourea SC (NH ₂) ₂ mL
CCTS-1	10	5	5	70
CCTS-2	10	5	5	80
CCTS-3	10	5	5	90

2.2 Synthesis of the Au/p-CCTS/n-SnO₂ diode

The SnO₂ thin layer (n type) was grown through a chemical spray pyrolysis technique, on a glass substrate heated to a temperature of 350 °C for 10 min at a solution flow of 4 mL/min. The SnO₂ solution was prepared by dissolving 0.05 M of tin II chloride SnCl₂ (99.9 %, Sigma Aldrich) in 40 mL of distilled water. The Cu₂CoSnS₄ absorbing layer with 80 mL of thiourea and a precursor concentration of 0.10 M has been synthesized with the chemical spray process. Before spraying, part of the SnO₂ substrate was isolated in order to make the electrical contacts. Afterwards the gold contacts were deposited by magnetron sputtering on CCTS/SnO₂ films. To summarize the fabrication of the diode, the structure of the fabricated device (SnO₂/CCTS/Au) is shown in Figure.1.

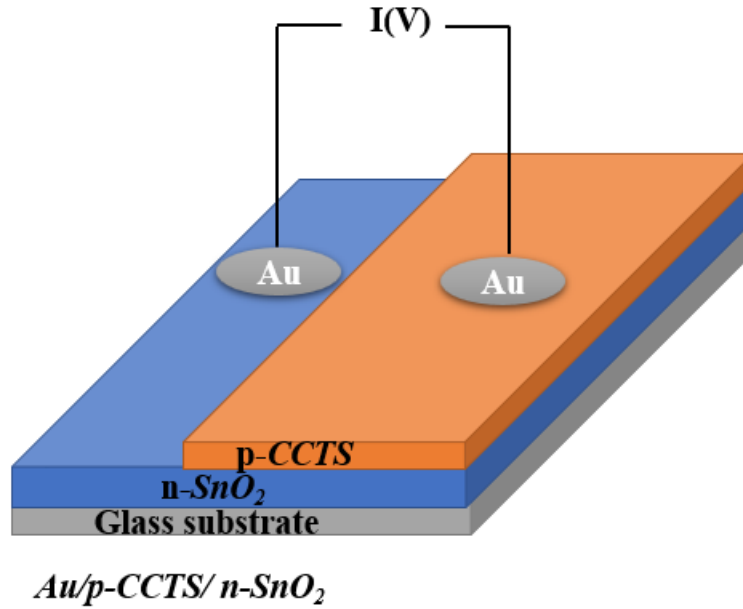


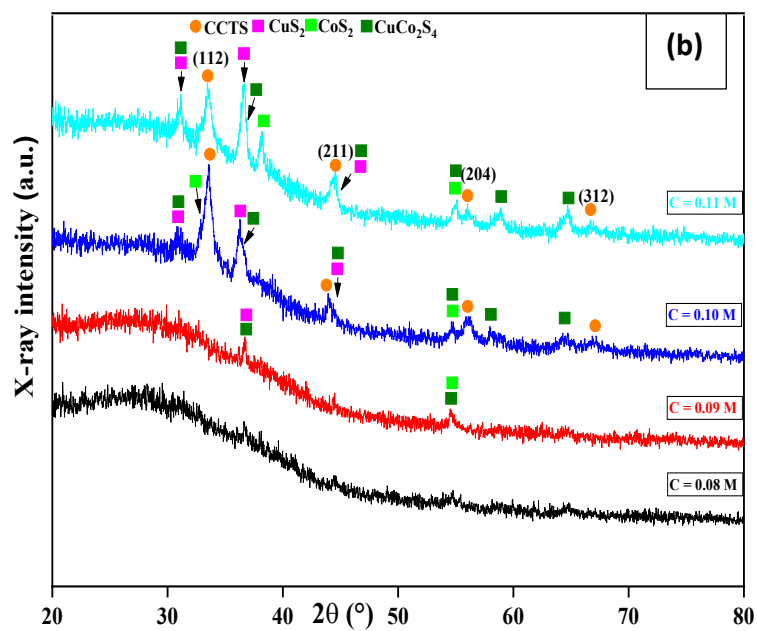
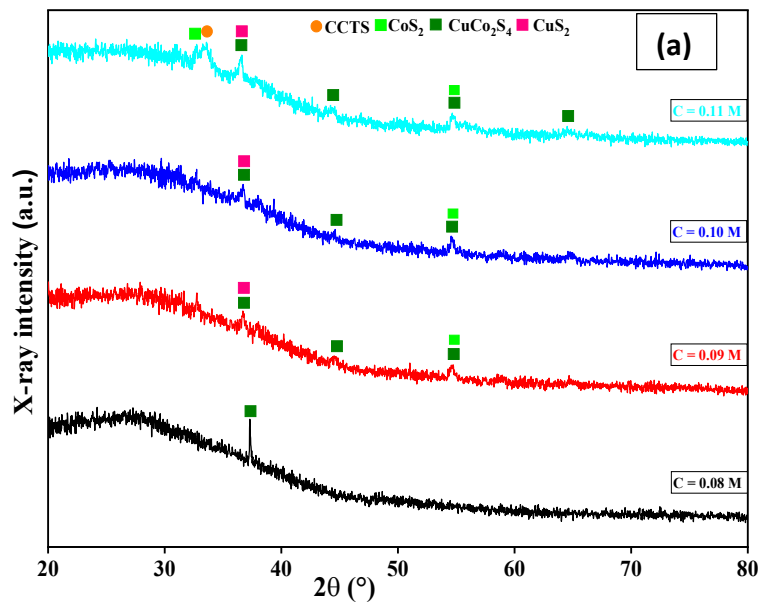
Figure. 1. The device structure of SnO₂/CCTS/Au thin film.

2.3 Characterization of CCTS thin films

The structural properties of CCTS thin films were analyzed using X-ray diffraction (XRD, Bruker D8 Focus) with Co-K_{α1+2} radiation ($\lambda = 1.7840 \text{ \AA}$) operated in the scanning angle 2θ from 20 to 80° (Bragg-Brentano configuration, 0.02° step) and Raman spectrometry (Jobin Yvon technology T 64000 spectrometer at room temperature under a 50 LF objective microscope, excited by a He-Ne laser). The surface morphology of the CCTS thin films was analyzed with a Field Emission Scanning Electron Microscopy (FE-SEM JEOL JSM-7800F). The cross-section observations were also carried out to estimate the coating thickness. The chemical composition of the films was estimated by Energy Dispersive Spectroscopy (EDS Quantax Bruker with XFLASH 6|30 detector). UV-Vis spectrophotometer (Shimadzu UV 3100S) was used to measure total transmittance and reflectance to determine optical parameters such as absorption coefficient and band gap energy. Resistivity measurements were carried out on the CCTS films at ambient temperature by the four-probe technique. The device is composed of a certified Jandel cell (Multi height probe, Jandel Engineering Limited), the factor shape is well known, and it is connected with an HP 3458A millimeter (Agilent) to measure electrical parameters whereas The current-voltage (I-V) characteristic of (Au/p-CCTS/ n-SnO₂) diode was performed at room temperature by means of Keithley 6517 electrometer under dark and light conditions.

3. Results and Discussion

3.1. Structural Characterization



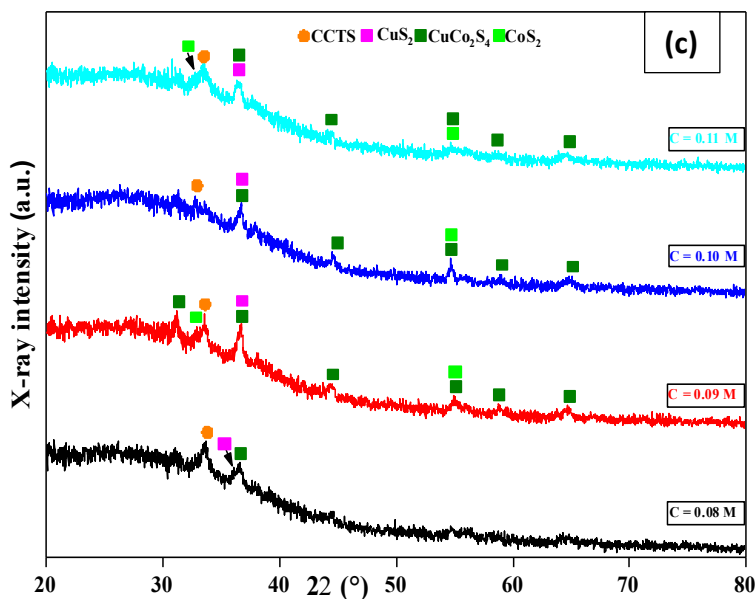


Figure.2. XRD diffractograms of CCTS thin films deposited at 320 °C with different precursors concentration and thiourea volume of 70 mL (a), 80 mL (b), and 90 mL (c).

Figure.2. (a) shows the XRD diffractograms of CCTS films prepared with 70 mL of thiourea and with various precursor concentrations. For precursor concentration up to 0.10 M, the film crystallization is really weak. Only the presence of secondary phases can be observable. The difference between the peaks and the background being low, their identification is rather tricky. Quaternary compounds are known to generate other phases as reported by [22] [24]. In reason with the relatively good agreement with the theoretical peak position, the CuCo_2S_4 is probable. Other compounds such as CuS_2 , or CoS_2 seems also possible. By increasing the precursor concentration to 0.11 M, the stannite CCTS phase is crystallized (space group I-42m).

Figure.2. (b) shows the XRD diffractograms of the CCTS thin films prepared with a thiourea volume of about 80 mL. A precursor concentration higher than 0.10 M is required to crystallize the stannite CCTS phase. The diffraction peaks coincide with the values reported by the Joint Committee on Powder Diffraction Standards (JCPDS) card number 00-026-0513, and the peaks positioned at 33.59, 43.99, 54.56 and 66.97° are assigned to the crystallographic plans: (112),

(202), (204) and (312), respectively. It is clear that the intensities of the diffraction lines are largely higher than the CCTS film prepared with 70 mL of thiourea volume, probably meaning a better crystallization of the stannite phase. The nature of secondary phases does not change, only their proportion increase. The X-ray diffractogram shows also the coexistence of secondary phases of cubic CuS_2 ($2\theta = 30.85, 36.19$ and 43.99° , JCPDS 03-065-4850), CoS_2 ($2\theta = 37.69$ and 54.65° , JCPDS 00-041-141) and CuCo_2S_4 ($2\theta = 30.85, 36.6, 58.41$ and 64.7° , JCPDS 00-002-0787). At a precursor concentration of 0.11 M, the relative X-ray diffraction intensities of the CCTS phase is lower compared to that of the CuS_2 secondary phase. The quality of the stannite and/or its proportion would be reduced.

The X-ray diffractograms of the CCTS films synthesized with 90 mL of thiourea are shown in Figure.2. (c). The crystallization of the stannite phase is observable for all precursor concentrations, with the coexistence of secondary phases such as CuS_2 , CuCo_2S_4 or CoS_2 .

The crystallization of the wanted stannite phase depends on both the precursor solution concentration and thiourea volume. While it is well known that a minimum of thiourea volume is necessary to crystallize stoichiometric sulfide compound, the required minimum is depending on the precursor solution concentration. Increasing the thiourea volume will lead to a larger stannite formation domain. However, the formation of a quality stannite structure seems only possible in a narrow domain of thiourea volume and precursor solution concentration, especially for thin films deposited at 80 ml and $C = 0.10-0.11$ M which will be the center of interest in the following parts.

The lattice parameters of the elaborated thin films were calculated using the Bragg formula and the interplanar distance equation [25]:

Bragg's law:

$$2d_{hkl} \sin \theta = n\lambda \quad (1)$$

Interplanar distance for a tetragonal symmetry:

$$d_{hkl} = \frac{a}{\sqrt{h^2 + k^2 + l^2 \frac{a^2}{c^2}}} \quad (2)$$

Where θ is the Bragg angle ($^\circ$), n is the diffraction order equal to 1, λ is the X-ray wavelength (0.17890 nm), h , k and l are the Miller indices of the crystallographic plane, and a and c are the lattice parameters (nm).

Furthermore, the microstructure study was further investigated with the determination of several parameters such as the crystallite size, the dislocation density, and the microstrain level. The average crystallite size D of the CCTS phase (see table 2) was calculated using the intense diffraction line (112) and using the Debye–Scherrer formula [26]:

$$D = \frac{0.9\lambda}{\beta \cos \theta} \quad (3)$$

Where β , θ , λ is the Full-Width at Half-Maximum (FWHM) assuming negligible instrumental width, the Bragg diffraction angle ($^\circ$) and the X-ray wavelength ($\lambda=1.78 \text{ \AA}$), respectively, and K is the so-called Scherrer constant. In order to define K , it is important to consider the crystallite shape, the distribution size, the indices of the diffraction line, and the actual definition used for β whether FWHM or integral [27]. K has a range between 0.62 and 2.08.

In this study, K is equal to 0.9. Furthermore, the microstrain in the crystallite or nanocrystal affects the width β , which needs to be taken into account in an accurate analysis. The width can be influenced by the alloy composition's spatial fluctuations [28].

The dislocation density (δ) is defined as the length of dislocation lines per unit volume. The dislocation density (δ) (see table 1) was calculated using this formula [29]:

$$\delta = \frac{1}{D^2} \quad (4)$$

The microstrain ε in the thin films is noticed due to crystal imperfections, dislocations, and point defects and is determined using the following equation [30]:

$$\varepsilon = \frac{\beta}{4 \tan(\theta)} \quad (5)$$

Table 2 presents the computed values of D, δ and ϵ obtained from XRD study of the CCTS thin films. The increase of the concentration has a moderate impact on the microstructure of the CCTS phase. Indeed, the crystallite size, the dislocation density or even the microstrain level stay of the same order of magnitude.

Table.2. Structural parameters of the CCTS thin films for 2 different precursor concentrations ($V_{th} = 80$ mL).

Precursor concentration (M)	Standard diffraction angle 2θ ($^\circ$)	Observed diffraction angle 2θ ($^\circ$)	FWHM ($^\circ$)	D (nm)	ϵ	δ (10^{-2}nm^{-2})
0.10	33.33	33.59	0.85	12	1.6	0.8
0.11	33.33	33.47	0.78	13	0.6	0.6

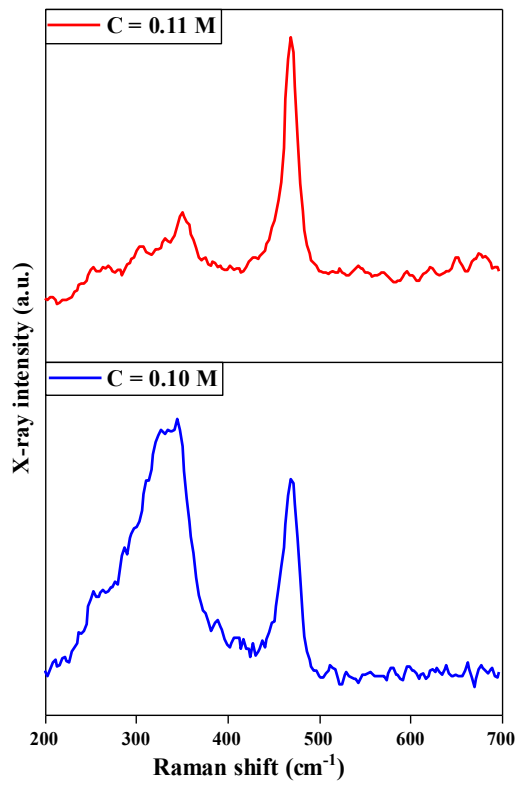


Figure.3. The Raman spectra of films deposited at 0.10 M and .011 M of precursor concentrations ($V_{th} = 80$ mL).

A Raman characterization technique was applied to thin films synthesized with precursor concentrations of 0.10 and 0.11 M over the range of 200 to 700 cm^{-1} (Figure 3). For a concentration of 0.10 M, Raman peaks located at 284, 325 and 344 cm^{-1} are consistent with specific vibrational modes of CCTS thin films reported [31] [32] [33]. Furthermore, the sharp peak with high intensity at 471 cm^{-1} can be attributed to the lattice vibration of copper sulfide [34] [35] [31]. The secondary phases of CuCo_2S_4 (CCS) and CoS_2 , which are clearly observed by XRD, are not detected in the Raman spectrum. As the precursor molarity increases, the characteristic peaks of CCTS strongly decrease, while the peak at 471 cm^{-1} related to copper sulfide phase is still intense in agreement with XRD observations and confirming the decrease of the proportion of the stannite CCTS phase with higher precursor solution concentration. The results of this study suggest that $C = 0.10$ M is the optimal concentration.

3.2. Chemical Composition Characterization

The average chemical composition of $\text{Cu}_2\text{CoSnS}_4$ thin films synthesized at different thiourea volumes was investigated by EDS analysis (see Table 4). As observed from this table, all CCTS thin layers exhibit a slight deficiency in Sn and enrichment in Cu. The Cu slight enrichment is consistent with the formation of Cu-based secondary phases (CuS_2 and CuCo_2S_4) as observed in XRD and Raman spectroscopy. In addition, the films are slightly under stoichiometric in sulfur except the film synthesized with a thiourea volume of 80 mL. The volume of thiourea was largely overdosed to compensate the sulfur evaporation during deposition on the hot substrate, but the increase of the thiourea volume does not lead to the sulfur excess. In the film The deviations from the stoichiometry (Cu-rich, Sn or S-deficiency) could lead to the formation of chemical defects in CCTS films that would act as electron trap states [11] [36], affecting the electrical properties of chalcogenide films [37]. These chemical defects would also inhibit the crystallization of the CCTS and lead to the formation of the secondary phases.

Table.4. Composition ratios of the CCTS thin films deposited at different thiourea volumes (0.10 M precursor concentration).

Thiourea volumes (mL)	Cu/(Cu+Co)	Cu/(Cu+Sn)	Co/(Co+Sn)	S/(S+Cu+Co+Sn)
Expected ratio from stoichiometry	0.70	0.70	0.50	0.50
70	0.66	0.73	0.57	0.36
80	0.69	0.75	0.56	0.48
90	0.67	0.74	0.58	0.40

3.5. Morphological characterization

The morphological characteristics of CCTS-based thin films deposited with different thiourea volume are evaluated using a scanning electron microscope. Figure.4 shows the topography of the CCTS thin films. It can be seen that the surface of the CCTS thin films is rather rough and compact. No voids or cracks are seen on the entire substrate. Coarse micrometric nodules can mainly be observed on the film surface synthesized with 70 and 90 mL of thiourea. Previous chemical measurements on the nodules reveal that they are rich in Cu and S [19] and would correspond to copper sulfide detected by Raman spectroscopy and X-ray diffraction. The film synthesized with a moderate volume of thiourea (80 mL) exhibits finer nodules (~ few hundreds nm) in addition to the larger nodules. The films thickness evolves from 0.6 to 1.1 and 1.4 μm depending on the thiourea volume, respectively.



Figure.4. Surface SEM images of CCTS thin films synthesized at different thiourea volumes (from left to right: 70, 80 and 90 mL) with 0.10 M precursor concentration.

3.6. Electrical characterizations:

Table.5. Electrical resistivity of CCTS thin films deposited at different thiourea volumes (C = 0.10 M).

Thiourea volumes (mL)	Electrical resistivity ($\Omega\cdot\text{cm}$)
70	$3.2 \cdot 10^{-2}$

80	$0.4 \cdot 10^{-2}$
90	$7.8 \cdot 10^{-4}$

The electrical resistivity of the CCTS thin films at room temperature was measured by the four-probe method. The electrical resistivity of films having the tetragonal stannite as main phase is about $0.4 \cdot 10^{-2} \Omega \cdot \text{cm}$. Takano et al. have reported an electrical resistivity of about $1.2 \cdot 10^{-4} \Omega \cdot \text{cm}$ at 300 K. Then the coexistence of the stannite with phases such as CuCo_2S_4 would explain the lower electrical resistivity [38]. The electrical resistivity for thiourea volume equal to 70 mL is $3.2 \times 10^{-2} \Omega \cdot \text{cm}$, which decrease to $7.8 \times 10^{-4} \Omega \cdot \text{cm}$ for a thiourea volume of 90 mL. Such behavior cannot be explained by the deviation from the stoichiometry in the stannite phase since the chemical composition of the film prepared with 90 mL is similar to that of the film synthesized with 70 mL. The decreases in electrical resistivity with increasing thiourea volume would be mainly ascribed to the presence of the secondary phases such as CuCo_2S_4 known for its thermoelectric properties.

3.7. Optical characterizations:

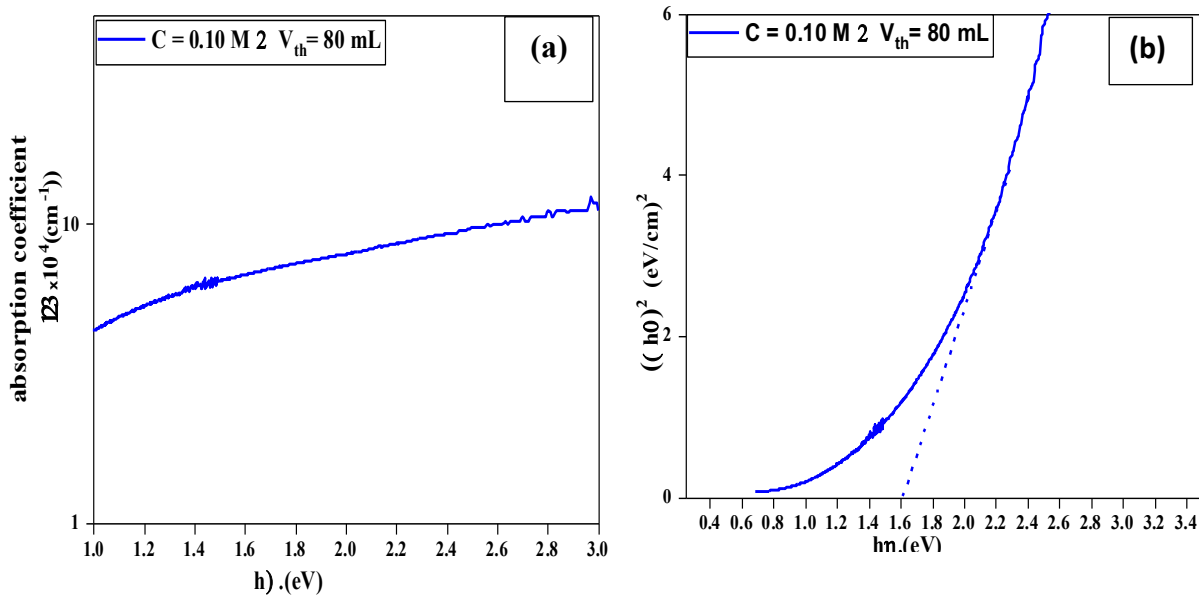


Figure.5. Optical parameters of CCTS thin films deposited at $C = 0.10 \text{ M}$ ($V_{\text{th}} = 80 \text{ mL}$) (substrate temperature $320 \text{ }^\circ\text{C}$); (a): Absorption coefficient spectrum, (b): Plot of $(ahv)^2$ versus $h\nu$.

The optical properties of the CCTS film prepared with 80 mL of thiourea and a precursor concentration of 0.10 M have been estimated by spectrophotometry (Figure.5). The absorption coefficient can be determined from the equation [16]:

$$\alpha = \frac{1}{d} \times \ln\left(\frac{1-R^2}{T}\right) \quad (6)$$

Where α is the absorption coefficient in cm^{-1} , d the film thickness in cm, R the total reflectance and T the total transmittance of the film. Figure 5.a shows the variation of the optical absorption coefficient as a function of the wavelength. The absorption coefficient is larger than 10^4 cm^{-1} in the visible solar spectrum, in agreement with the reported values in the literature [9]. The absorption coefficient almost reaches 10^5 cm^{-1} at 500 nm (2.48 eV) for the wavelength corresponding to the maximal irradiance of the solar spectrum. Furthermore, since CCTS is a direct bandgap semiconductor, the optical absorption coefficient (α) and the bandgap (E_g) are related by the following relationship [2]:

$$\alpha h\nu = A(h\nu - E_g)^n \quad (7)$$

The bandgap E_g of the CCTS thin film deposited at $C = 0.10 \text{ M}$ and $V_{\text{th}} = 80 \text{ mL}$ is found to be $\sim 1.6 \text{ eV}$ by extrapolating the linear portion of the plot of $(\alpha h\nu)$ vs. photon energy ($h\nu$) to zero, as shown in the Figure.5.b. This value is slightly higher than that reported by other research groups ($E_g \sim 1.23\text{-}1.45 \text{ eV}$) [35] [15], [39]. The formation of secondary phases based on sulfide compounds with bandgap values higher than that of the CCTS phase (CuS_2 1.87 eV or CoS_2 2.22 eV) would explain the observed higher bandgap energy range.

4. Study of electrical features of the Au/p-CCTS/n-SnO₂ diode

4.1. Structural, optical and morphological properties of n type SnO₂ film

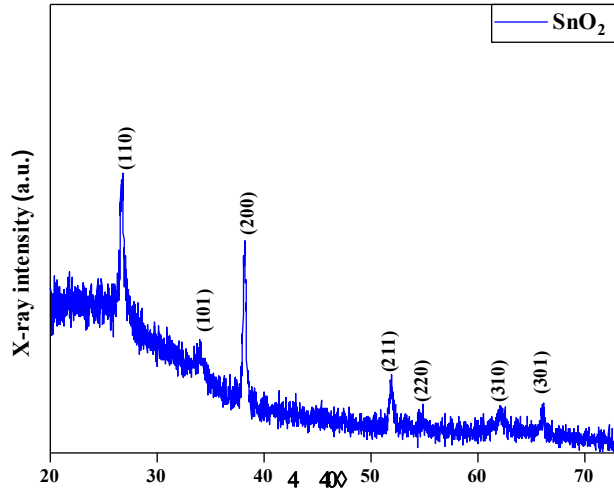


Figure.6. XRD pattern of SnO₂ thin film.

The XRD diffractogram of SnO₂ thin film is shown in Figure 6. The main peaks observed at 26.7 °, 33.9 °, 37.9 °, 51.6 °, 54.7 °, 61.7 ° and 65.6 ° are, respectively, assigned to (110), (101), (200), (211), (220), (310) and (301) planes of the tetragonal rutile structure of the SnO₂. The transmission and reflectance spectra of the SnO₂ thin film are shown in Figure. 7.a. and b. The SnO₂ film exhibits a high transmittance 80 % in the NIR as it expected from a transparent conductor oxide such as SnO₂. The reflection is low and remains between 15 and 20 %. Figure 7c shows a plot of $(\alpha h\nu)^2$ vs $h\nu$ and extrapolation of the linear part onto the $h\nu$ -axis to obtain the optical bandgap energy. This value for the thermally sprayed SnO₂ film is 3.6 eV, which is consistent with the literature [40]. Figure 8 shows the SEM surface of the SnO₂ thin film. The SnO₂ surface is compact, homogenous and dense.

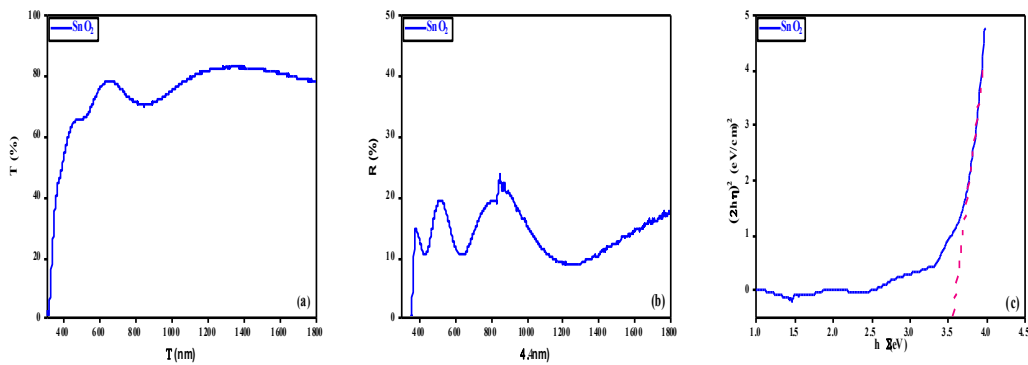


Figure 7 (a) and (b) Transmission and reflection spectra (c) Plot of $(ahv)^2$ versus (hv) of SnO_2 thin film.

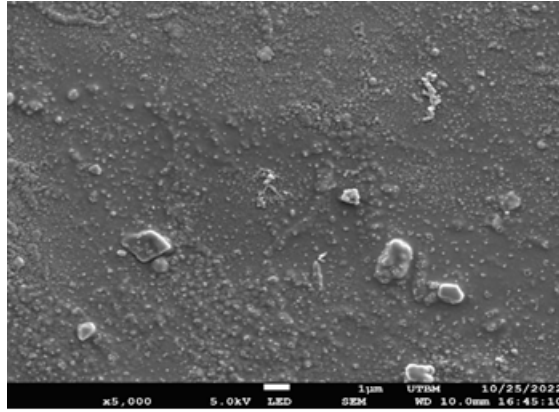


Figure 8. Micrograph of the surface of the sprayed SnO_2 thin film.

4.2 Electrical properties: current–voltage (I–V) characteristics

4.2.1. Dark current–voltage characterization

Several methods can be used to determine the diode barrier parameter, photoelectron spectroscopy, current-voltage (I-V) analysis, capacitance-voltage (C-V) analysis, and activation energy method [41]. The I-V analysis method is the simplest of all methods, as it directly measures the voltage and provides direct information about the nature of the barrier generated at the interface.

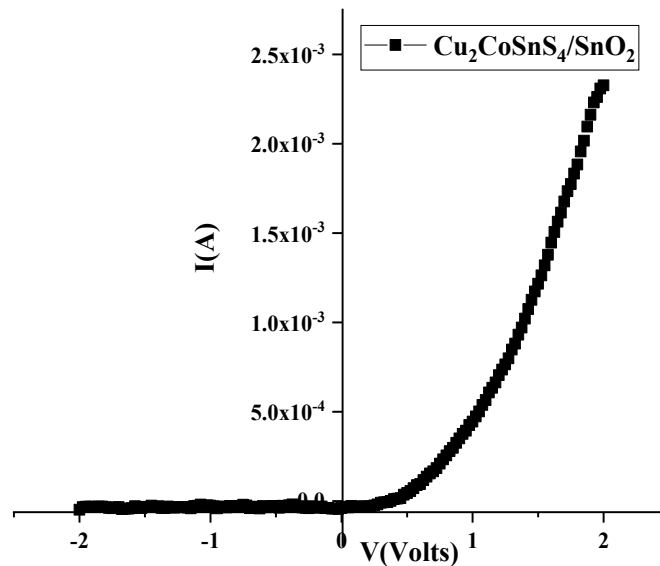


Figure.9. The experimental current–voltage characteristics of the Au/p-CCTS/ n-SnO₂ at room temperature in dark condition.

Figure.9 shows the experimental bias current–voltage (I–V) characteristics of the Au/Cu₂CoSnS₄/SnO₂ at room temperature. These I–V characteristics were analyzed using standard thermionic emission theory. According to this theory, the current is expressed by the following equation [42] [43]:

$$I = I_s \left[\frac{q}{nKT} (V - R_s I) - 1 \right] \quad (8)$$

where n is the diode ideality factor, q is the electrical charge of an electron ($-1.6 \cdot 10^{-19}$ C), K is Boltzmann's constant ($1,38 \cdot 10^{-23}$ J K⁻¹), T is the absolute temperature in Kelvin (298 K), V is the applied voltage in V, R_s is the series resistance (Ohm) and I₀ is the saturation current in A. As shown in Figure.9, the rectifying of the curve confirms that this junction behaves like a diode.

The saturation current I_s is determined by extrapolating the linear region of the forward-bias semi log I–V curves to the zero applied voltage (V = 0), as illustrated in figure 10 and referring to the logarithmic form 8 and 9. Then, the calculated value of I_s from the intercept of ln I = f(V) plot at V = 0 is found to be about $5 \cdot 10^{-6}$ A. A similar result was observed in CZTS and CNTS chalcogenides structures that is analogously with CCTS structure [44] [45] [46].

$$\ln(I) = \ln(I_s) + \frac{q}{nKT} (V - R_s I) \quad (9)$$

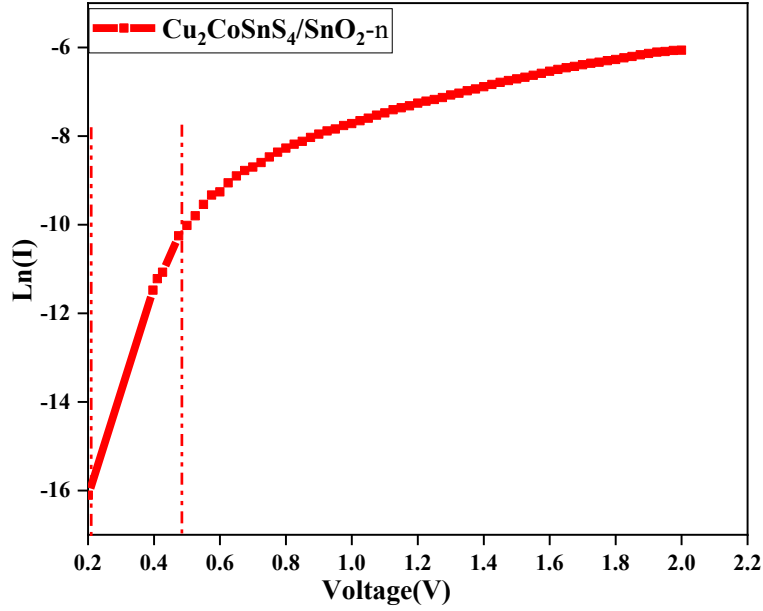


Figure.10. Variation of $\ln(I)$ versus voltage (V) in direct polarization of the Au/p-CCTS/ n-SnO₂.

The ideality factor n measures the conformance of a real diode to the pure thermionic emission theory when n is unity (ideal diode). However, n is usually greater than 1. Moreover, deviations of the experimental I–V data from the ideal thermionic model are explained by this parameter, also allowing a deeper understanding of the contributions of other current transport mechanisms [47] [48].

It can be determined from the slope of the linear region of the forward bias I–V characteristics using the following equation [49] [50]:

$$n = (q / KT) * [dV / d \ln(I)] \quad (9)$$

For an ideal diode, ideality factor equals to 1, but according to our result, experimental value of n is 3. This indicates that the n value is higher than ideal and the increase in the ideality factor could be due to several effects, such as film thickness non-uniformity, interfacial states, series resistance, tunneling process and randomness of interfacial charge distribution homogeneity [51]. However, the high ideality factor is often attributed to defect states with in the semiconductor bandgap [52]. This result is a little far with that found by ELRADAF et al [53], Touati et al [54], Oueslati et al [55] and Mahjoubi et al [44].

The series resistance R_s is a very important parameter that affects the solar cell performance. In fact, high series resistance significantly reduces the fill factor and, as a result, the efficiency of the cell. Series resistance can be expressed by Cheung's function given by:

$$\frac{dV}{d \ln(I)} = R_s I + n \frac{KT}{q} \quad (10)$$

Figure 11 illustrates the variation of $\frac{dV}{d \ln(I)}$ versus the current I for the Au/Cu₂CoSnS₄/SnO₂ diode structure. It has a linear behavior and the R_s series resistance can be readily obtain from the slope which is evaluated to be 689 Ω .

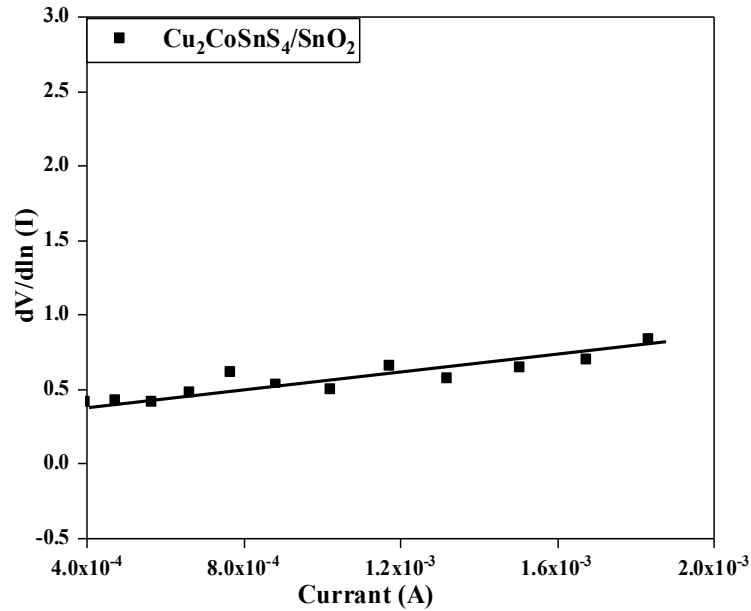


Figure.11. The experimental $\frac{dV}{d \ln(I)}$ versus I plot of the diode structure of the Au/p-CCTS/ n-SnO₂

The shunt resistance R_{sh} is also an important parameter to improve the performance of the diode device. It reflects the number of manufacturing defects rather than the poor junction design. The

high value of R_{sh} in a junction indicate the good quality of the investigated diode. The presence of high R_{sh} results a decrease of impurity and defects in junction materials, furthermore it conduct to decrease the leakage current [56] [57].

The shunt resistance can be concluded from the plot of the diode junction resistance, $R_J(V)$ [58], where $R_J = \partial V / \partial I$. A plot of R_J against V is illustrated in the Figure shown below for the Au/p-CCTS/ n-SnO₂ diode. Then, the obtained value of R_{sh} is equal 1.56 M Ω . This result is in agreement with that found by M.M. El-Nahass, et al. [59].

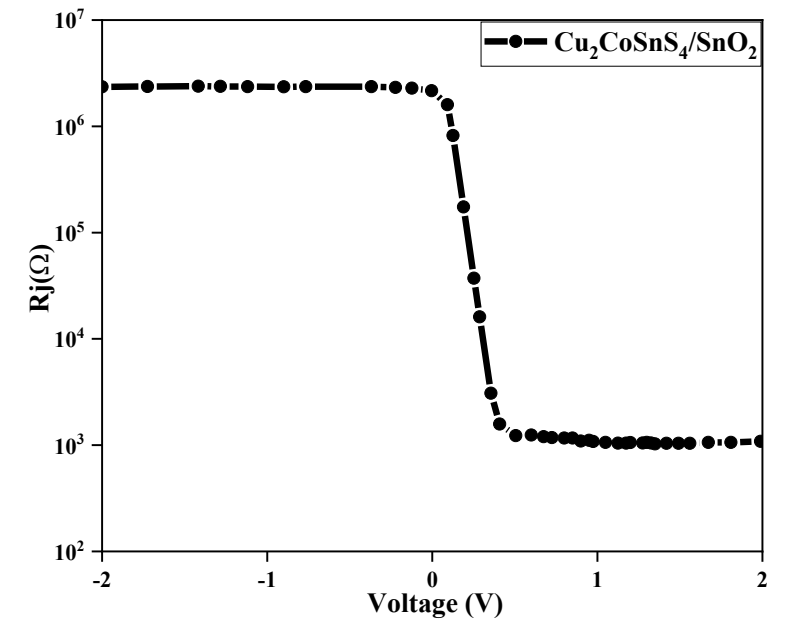


Figure.12. Junction resistance, R_J , versus V of the diode structure of the Au/p-CCTS/ n-SnO₂

The table below shows a comparative overview between our obtained results and other researches.

Table.6. Summary of the device parameters estimated from Cheung's function for the different diodes

Device structure	Saturation current, I_s (A)	Ideality factor, n	Series resistance, R_s (Ω)

Au/p-CCTS/ n-SnO₂	$5*10^{-6}$	3	689
Al/n-Si/Cu₂CoSnS₄/Au [53]	-----	[2.06-2.68]	[133-205]
ZnS/CZTS/Au [60]	$1.27*10^{-6}$	5.9	2000
Mo/ CZTS/Al [61]	$[1.93-2.11] *10^{-6}$	[5.43-5.74]	[2099-2280]
Ag/p-Cu₂NiSnS₄ [45]	$8.24*10^{-6}$	2.23	261
Al/p-Cu₂ZnSnS₄ [54]	$0.829*10^{-6}$	1.56	21.61

The overall results of the device parameters of our diode presented in Table 6 are in good agreement with the research results reported in [53] [45] [54] [60] [54] . All authors are agreed that the increase of the series resistance can explain the large ideality factor. Furthermore, the high value of series resistance of the Au/Cu₂CoSnS₄/SnO₂ diode attributed to the non-ideality of the system and may be attributed the high resistivity of the secondary phases like CuS₂ [55].

4.2.2. Illumination Current–Voltage Characterization:

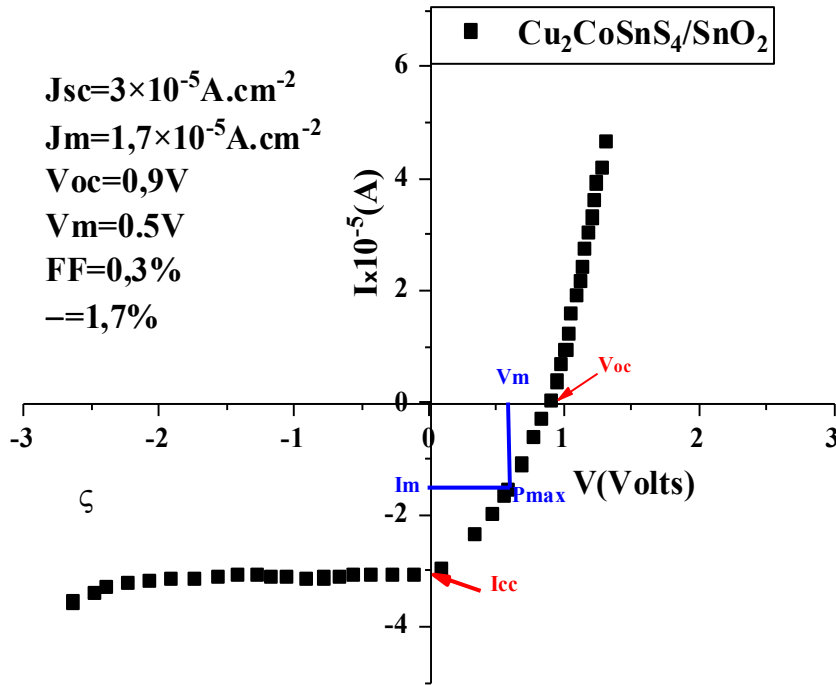


Figure.13. The I–V characteristics of the Au/ Cu₂CoSnS₄/SnO₂ diode under illumination (total active area $1 \times 1 \text{ cm}^2$)

Photovoltaic analysis of Au/Cu₂CoSnS₄/SnO₂ diode was studied by determining the I–V characteristics under illumination condition. The illuminated I–V curve of the Au/Cu₂CoSnS₄/SnO₂ diode is presented in Figure.13. Moreover, the photovoltaic constants of the prepared diode as the short-circuit current density $J_{sc}= 3 \times 10^{-5} \text{ A.cm}^{-2}$, maximum current density $J_m = 1.7 \times 10^{-5} \text{ A.cm}^{-2}$, the open-circuit voltage $V_{OC}= 0.9 \text{ V}$, maximum voltage $V_m = 0.5 \text{ V}$ and the efficiency were estimated via this plot. The cell efficiency of the device ρ and fill factor of the Au/Cu₂CoSnS₄/SnO₂ diode have been evaluated according to the below relations:

$$\rho = \frac{P_{\max}}{P_{in}} = \frac{V_{oc} * J_{sc}}{P_{in}} * 100\% \quad (11)$$

$$FF = \frac{V_m * J_m}{V_{oc} * J_{sc}} \quad (12)$$

where P_{in} (watt) denotes the input energy from the sun, P_{max} denotes the output energy from the device, FF is the fill factor, I_{cc} is the short-circuit current and V_{oc} represents the open-circuit voltage. The magnitudes of the FF and the ρ of the Au/Cu₂CoSnS₄/SnO₂ diode were 0.3 % and 1.7 % respectively. These results are not very close with those found by Drissi et al [56] and EL Radaf et al [53] . this obtained result seems like cause of the coexistence of the secondary phases.

5. Conclusions

In this study, chalcogenide Cu₂CoSnS₄ thin films have been successfully synthesized by spray pyrolysis on glass substrate at ambient air and by using distilled water as a solvent. The structural properties of deposited CCTS thin films at different precursor concentrations (from 0.08 to 0.11 M) and thiourea volumes were examined in detail. While the crystallization of the stannite CCTS phase is possible in a large domain of precursor concentration and thiourea volume, this comes with the formation of secondary compounds based on sulfur resulting in a relatively poor crystallization of the wanted stannite phase. It is also shown that a decrease in precursor concentration needs a higher volume of thiourea in reducing the crystallization domain. The crystallization of quality stannite film can be succeeded in a limited range of precursor concentration and thiourea volume. This study revealed that the depositing CCTS thin film at $C = 0.10$ M and $V_{th} = 80$ mL results in a stannite structure, with a limited crystallization of secondary phases. The electrical resistivity is about 10^{-2} Ω .cm at room temperature. The absorption coefficient almost reaches 10^5 cm^{-1} for wavelength corresponding to the maximal irradiance of the solar spectrum. The use of an inexpensive and environmentally friendly process for the synthesis of solar energy absorbing thin film is demonstrated, but requires a relatively precise control of the solution preparation to form a stannite CCTS film with limited secondary phase formation and stoichiometry deviation. Then our demonstrated application leads us to conclude that the CCTS is a good promotor for preparing thin film solar cells with p-CCTS as an absorber layer by mean of spray pyrolysis technique.

Acknowledgements:

The authors wish to acknowledge the Tunisian Ministry of Higher Education and Scientific Research for financial support for this study. This work was performed within his FEMTO-ST SURFACE platform.

Author contributions:

FH: contributed to conceptualization, investigation, Writing original draft, Visualization. EA: Data curation, formal analysis- editing, writing review and software. NB and PB supervision resources- project administration.

Funding:

The authors declare that no competing financial interests exist.

Data availability:

Data sharing is not relevant to this article as no datasets were generated or analyzed in the current study.

Declarations:

Conflict of interest: The authors claim that they've no conflict of interest.

Ethical approval: The authors declare that this article does not contain any studies of human intervention by the authors. Results fit well in the context of previous and existing studies

References

- [1] X. Zhang *et al.*, "Crystal phase-controlled synthesis of Cu₂FeSnS₄ nanocrystals with a band gap of around 1.5 eV," *Chem. Commun.*, vol. 48, no. 41, p. 4956, 2012, doi: 10.1039/c2cc31648j.
- [2] M. Krishnaiah, Y. J. Jeong, R. K. Mishra, M. J. Kim, J. Song, and S. H. Jin, "Temperature-Time profile effects on evolution of physical and electronic properties in visible light Cu₂CoSnS₄ photodetectors," *Mater. Sci. Semicond. Process.*, vol. 121, p. 105443, 2021.
- [3] B. Murali and S. B. Krupanidhi, "Facile synthesis of Cu₂CoSnS₄ nanoparticles exhibiting red-edge-effect: Application in hybrid photonic devices," *J. Appl. Phys.*, vol. 114, no. 14, p. 144312, Oct. 2013, doi: 10.1063/1.4825070.
- [4] P. S. Maldar *et al.*, "Fabrication of Cu₂CoSnS₄ thin films by a facile spray pyrolysis for photovoltaic application," *Sol. Energy*, vol. 158, pp. 89–99, Dec. 2017, doi: 10.1016/j.solener.2017.09.036.
- [5] M. Krishnaiah, P. Bhargava, and S. Mallick, "Low-temperature synthesis of Cu₂CoSnS₄ nanoparticles by thermal decomposition of metal precursors and the study of its structural, optical

- and electrical properties for photovoltaic applications," *RSC Adv.*, vol. 5, no. 117, pp. 96928–96933, 2015, doi: 10.1039/C5RA18679J.
- [6] M. Krishnaiah, R. K. Mishra, S. G. Seo, S. H. Jin, and J. T. Park, "Highly crystalline, large grain Cu₂CoSnS₄ films with reproducible stoichiometry via direct solution spin coating for optoelectronic device application," *Ceram. Int.*, vol. 45, no. 9, pp. 12399–12405, 2019.
- [7] F. Harrathi, E. Aubry, S. Dridi, P. Briois, and N. Bitri, "Effect of the substrate temperature on the synthesis of the Cu₂CoSnS₄ thin films by spray pyrolysis for solar cells devices," *J. Mater. Sci. Mater. Electron.*, vol. 34, no. 4, 2023, doi: 10.1007/s10854-022-09720-6.
- [8] D. Zhang *et al.*, "Multi-cations compound Cu₂CoSnS₄: DFT calculating, band engineering and thermoelectric performance regulation," *Nano Energy*, vol. 36, pp. 156–165, 2017.
- [9] C. Xiao *et al.*, "Magnetic ions in wide band gap semiconductor nanocrystals for optimized thermoelectric properties," *Mater Horiz*, vol. 1, no. 1, pp. 81–86, 2014, doi: 10.1039/C3MH00091E.
- [10] F. Ozel, E. Aslan, B. Istanbulu, O. Akay, and I. H. Patir, "Photocatalytic hydrogen evolution based on Cu₂ZnSnS₄, Cu₂NiSnS₄ and Cu₂CoSnS₄ nanocrystals," *Appl. Catal. B Environ.*, vol. 198, pp. 67–73, 2016.
- [11] K. Mokurala, S. Mallick, and P. Bhargava, "Alternative quaternary chalcopyrite sulfides (Cu₂FeSnS₄ and Cu₂CoSnS₄) as electrocatalyst materials for counter electrodes in dye-sensitized solar cells," *J. Power Sources*, vol. 305, pp. 134–143, 2016.
- [12] M. K. Gonc, E. Aslan, F. Ozel, and I. Hatay Patir, "Dye-Sensitized Cu₂XSnS₄ (X=Zn, Ni, Fe, Co, and Mn) Nanofibers for Efficient Photocatalytic Hydrogen Evolution," *ChemSusChem*, vol. 9, no. 6, pp. 600–605, Mar. 2016, doi: 10.1002/cssc.201501661.
- [13] F. López-Vergara, A. Galdámez, V. Manríquez, and G. González, "Crystal structure and Raman scattering characterization of Cu₂Fe_{1-x}Co_xSnS₄ chalcogenide compounds," *Solid State Sci.*, vol. 49, pp. 54–60, Nov. 2015, doi: 10.1016/j.solidstatesciences.2015.09.010.
- [14] X. Zhang, N. Bao, B. Lin, and A. Gupta, "Colloidal synthesis of wurtzite Cu₂CoSnS₄ nanocrystals and the photoresponse of spray-deposited thin films," *Nanotechnology*, vol. 24, no. 10, p. 105706, 2013.
- [15] P. S. Maldar, A. A. Mane, S. S. Nikam, S. D. Dhas, and A. V. Moholkar, "Spray deposited Cu₂CoSnS₄ thin films for photovoltaic application: Effect of film thickness," *Thin Solid Films*, vol. 709, p. 138236, 2020.
- [16] H. Y. S. Al-Zahrani, "Synthesis, optical and optoelectrical analysis of the Cu₂CoSnS₄ thin films as absorber layer for thin-film solar cells," *J. Mater. Sci. Mater. Electron.*, vol. 31, no. 9, pp. 6900–6909, 2020.
- [17] S. Dridi, E. Aubry, N. Bitri, F. Chaabouni, and P. Briois, "Growth and Characterization of Cu₂MnSnS₄ Thin Films Synthesized by Spray Pyrolysis under Air Atmosphere," *Coatings*, vol. 10, no. 10, p. 963, 2020.
- [18] D. Perednis and L. J. Gauckler, "Thin Film Deposition Using Spray Pyrolysis," *J. Electroceramics*, vol. 14, no. 2, pp. 103–111, Mar. 2005, doi: 10.1007/s10832-005-0870-x.
- [19] C. H. Chen, E. M. Kelder, and J. Schoonman, "Effects of additives in electrospraying for materials preparation," *J. Eur. Ceram. Soc.*, vol. 18, no. 10, pp. 1439–1443, 1998.
- [20] S. G. Nilange, N. M. Patil, and A. A. Yadav, "Influence of precursor thiourea contents on the properties of spray deposited Cu₂FeSnS₄ thin films," *Phys. B Condens. Matter*, vol. 570, pp. 73–81, 2019.
- [21] M. Messaoudi, M. S. Aida, N. Attaf, and S. Satta, "SnS thin films deposition by spray pyrolysis: solvent influence," *Int. J. Chalcogenide Lett.*, vol. 16, no. 4, pp. 157–162, 2019.
- [22] M. Beraich *et al.*, "Preparation and characterization of Cu₂CoSnS₄ thin films for solar cells via co-electrodeposition technique: Effect of electrodeposition time," *Optik*, vol. 193, p. 162996, Sep. 2019, doi: 10.1016/j.ijleo.2019.162996.

- [23] S. G. Nilange, N. M. Patil, and A. A. Yadav, "Growth and characterization of spray deposited quaternary Cu₂FeSnS₄ semiconductor thin films," *Phys. B Condens. Matter*, vol. 560, pp. 103–110, 2019.
- [24] M. Krishnaiah, A. Kumar, J. Song, and S. H. Jin, "Cu/(Co+Sn) ratio effects on physical and photodetective properties for visible light absorbing Cu₂CoSnS₄ nanoparticles via a one-pot hydrothermal process," *J. Alloys Compd.*, vol. 847, p. 156174, Dec. 2020, doi: 10.1016/j.jallcom.2020.156174.
- [25] J. Kacher, C. Landon, B. L. Adams, and D. Fullwood, "Bragg's Law diffraction simulations for electron backscatter diffraction analysis," *Ultramicroscopy*, vol. 109, no. 9, pp. 1148–1156, Aug. 2009, doi: 10.1016/j.ultramic.2009.04.007.
- [26] P. Scherrer, "Bestimmung der Grosse und inneren Struktur von Kolloidteilchen mittels Rontgenstrahlen," *Nach Ges Wiss Gottingen*, vol. 2, pp. 8–100, 1918.
- [27] J. I. Langford and A. J. C. Wilson, "Scherrer after sixty years: a survey and some new results in the determination of crystallite size," *J. Appl. Crystallogr.*, vol. 11, no. 2, pp. 102–113, 1978.
- [28] V. Uvarov and I. Popov, "Metrological characterization of X-ray diffraction methods for determination of crystallite size in nano-scale materials," *Mater. Charact.*, vol. 58, no. 10, pp. 883–891, 2007.
- [29] G. K. Williamson and R. E. Smallman, "III. Dislocation densities in some annealed and cold-worked metals from measurements on the X-ray debye-scherrer spectrum," *Philos. Mag.*, vol. 1, no. 1, pp. 34–46, Jan. 1956, doi: 10.1080/14786435608238074.
- [30] I. M. El Radaf, S. S. Fouad, A. M. Ismail, and G. B. Sakr, "Influence of spray time on the optical and electrical properties of CoNi₂S₄ thin films," *Mater. Res. Express*, vol. 5, no. 4, p. 046406, 2018.
- [31] M. Oubakalla *et al.*, "Effects of copper concentration on the properties of Cu₂CoSnS₄ thin films co-electrodeposited on the FTO substrate," *J. Mater. Sci. Mater. Electron.*, vol. 33, no. 15, pp. 12016–12025, 2022.
- [32] M. K. Sahoo, M. Gusain, S. Thangriyal, R. Nagarajan, and G. R. Rao, "Energy storage study of trimetallic Cu₂M₂SnS₄ (M: Fe, Co, Ni) nanomaterials prepared by sequential crystallization method," *J. Solid State Chem.*, vol. 282, p. 121049, Feb. 2020, doi: 10.1016/j.jssc.2019.121049.
- [33] M. A. Ahmed, N. A. Bakr, and A. A. Kamil, "Synthesis and characterization of chemically sprayed Cu₂CoSnS₄ Thin Films," *Chalcogenide Lett.*, vol. 16, no. 5, pp. 231–239, 2019.
- [34] M. Ishii, K. Shibata, and H. Nozaki, "Anion Distributions and Phase Transitions in Cu_{1-x}Se_x (x = 0-1) Studied by Raman Spectroscopy," *J. Solid State Chem.*, vol. 105, no. 2, pp. 504–511, Aug. 1993, doi: 10.1006/jssc.1993.1242.
- [35] T. Hurma and S. Kose, "XRD Raman analysis and optical properties of CuS nanostructured film," *Optik*, vol. 127, no. 15, pp. 6000–6006, Aug. 2016, doi: 10.1016/j.ijleo.2016.04.019.
- [36] M. Kumar, A. Dubey, N. Adhikari, S. Venkatesan, and Q. Qiao, "Strategic review of secondary phases, defects and defect-complexes in kesterite CZTS–Se solar cells," *Energy Environ. Sci.*, vol. 8, no. 11, pp. 3134–3159, 2015, doi: 10.1039/C5EE02153G.
- [37] G. Y. Senguler, E. K. Narin, S. B. Lisesivdin, and T. Serin, "Effect of sulfur concentration on structural, optical and electrical properties of Cu₂CoSnS₄ absorber film for photovoltaic devices," *Phys. B Condens. Matter*, vol. 648, p. 414424, Jan. 2023, doi: 10.1016/j.physb.2022.414424.
- [38] J.-M. Xu, X.-C. Wang, and J.-P. Cheng, "Supercapacitive Performances of Ternary CuCo₂S₄ Sulfides," *ACS Omega*, vol. 5, no. 3, pp. 1305–1311, Jan. 2020, doi: 10.1021/acsomega.9b03865.
- [39] X. Zhang, N. Bao, B. Lin, and A. Gupta, "Colloidal synthesis of wurtzite Cu₂CoSnS₄ nanocrystals and the photoresponse of spray-deposited thin films," *Nanotechnology*, vol. 24, no. 10, p. 105706, Mar. 2013, doi: 10.1088/0957-4484/24/10/105706.

- [40] P. S. Patil, R. K. Kawar, T. Seth, D. P. Amalnerkar, and P. S. Chigare, "Effect of substrate temperature on structural, electrical and optical properties of sprayed tin oxide (SnO₂) thin films," *Ceram. Int.*, vol. 29, no. 7, pp. 725–734, 2003.
- [41] A. A. M. Farag, I. S. Yahia, and M. Fadel, "Electrical and photovoltaic characteristics of Al/n-CdS Schottky diode," *Int. J. Hydrog. Energy*, vol. 34, no. 11, pp. 4906–4913, 2009.
- [42] A. Keffous *et al.*, "Effect of series resistance on the performance of high resistivity silicon Schottky diode," *Appl. Surf. Sci.*, vol. 218, no. 1–4, pp. 337–343, 2003.
- [43] R. C. Anderson, R. S. Muller, and C. W. Tobias, "Investigations of the electrical properties of porous silicon," *J. Electrochem. Soc.*, vol. 138, no. 11, p. 3406, 1991.
- [44] S. Mahjoubi, N. Bitri, E. Aubry, F. Chaabouni, and P. Briois, "Back contact nature effect on the CZTS/ZnS based heterojunction," *Appl. Phys. A*, vol. 128, no. 5, p. 380, 2022.
- [45] P. R. Ghediya *et al.*, "Electrical properties of Ag/p-Cu₂NiSnS₄ thin film Schottky diode," *Mater. Today Commun.*, vol. 28, p. 102697, 2021.
- [46] F. Z. Boutebakh, M. L. Zeggar, N. Attaf, and M. S. Aida, "Electrical properties and back contact study of CZTS/ZnS heterojunction," *Optik*, vol. 144, pp. 180–190, 2017.
- [47] F. Jabli, H. Mosbahi, M. Gassoumi, C. Gaquierrec, M. A. Zaidi, and H. Maaref, "Electron/transport in (Mo/Au)/AlGaIn/GaN Schottky diode," *IOSR J Appl PhysIOSR-JAP*, vol. 6, pp. 27–34, 2014.
- [48] S. Alialy, H. Tecimer, H. Uslu, and Ş. Altındal, "A comparative study on electrical characteristics of Au/N-Si Schottky diodes, with and without Bi-doped PVA interfacial layer in dark and under illumination at room temperature," *J Nanomed Nanotechol*, vol. 4, no. 3, p. 1000167, 2013.
- [49] N. Tuğluoğlu, S. Karadeniz, M. Şahin, and H. Şafak, "Temperature-dependent barrier characteristics of Ag/p-SnSe Schottky diodes based on I–V–T measurements," *Semicond. Sci. Technol.*, vol. 19, no. 9, p. 1092, 2004.
- [50] S. Karadeniz, N. Tugluoglu, M. Şahin, and H. Şafak, "Series resistance calculation for Ag contacts on single crystal layered p-SnS and p-SnSe compound semiconductors in the wide temperature range," *Microelectron. Eng.*, vol. 81, no. 1, pp. 125–131, 2005.
- [51] A. A. M. Farag and I. S. Yahia, "Rectification and barrier height inhomogeneous in Rhodamine B based organic Schottky diode," *Synth. Met.*, vol. 161, no. 1–2, pp. 32–39, 2011.
- [52] J. H. Werner and H. H. Güttler, "Barrier inhomogeneities at Schottky contacts," *J. Appl. Phys.*, vol. 69, no. 3, pp. 1522–1533, 1991.
- [53] I. M. El Radaf, H. I. Elsaedy, H. A. Yakout, and M. T. El Sayed, "Junction parameters and electrical characterization of the Al/n-Si/cu₂CoSnS₄/au Heterojunction," *J. Electron. Mater.*, vol. 48, pp. 6480–6486, 2019.
- [54] R. Touati, I. Trabelsi, M. B. Rabeh, and M. Kanzari, "Structural and electrical properties of the Al/p-Cu₂ZnSnS₄ thin film schottky diode," *J. Mater. Sci. Mater. Electron.*, vol. 28, pp. 5315–5322, 2017.
- [55] H. Oueslati, K. Nefzi, M. B. Rabeh, and M. Kanzari, "Structural, morphological and electrical properties of the Al/p-Cu₂FeSnS₄ thin film Schottky diode grown by two method," *Mater. Lett.*, vol. 273, p. 127908, 2020.
- [56] I. M. El Radaf and M. S. El-Bana, "Synthesis and characterization of the CuSbSe₂/n-Si heterojunction: electrical and photovoltaic characterizations," *Phys. B Condens. Matter*, vol. 584, p. 412067, 2020.
- [57] S. Chatterjee and A. J. Pal, "A solution approach to p-type Cu₂FeSnS₄ thin-films and pn-junction solar cells: role of electron selective materials on their performance," *Sol. Energy Mater. Sol. Cells*, vol. 160, pp. 233–240, 2017.
- [58] S. Darwish, A. S. Riad, and H. S. Soliman, "Electrical conductivity and the effect of temperature on photoconduction of n-ZnSe/p-Si rectifying heterojunction cells," *Semicond. Sci. Technol.*, vol. 11, no. 1, p. 96, 1996.

- [59] M. M. El-Nahass, K. F. Abd-El-Rahman, A. A. M. Farag, and A. A. A. Darwish, "Photovoltaic properties of NiPc/p-Si (organic/inorganic) heterojunctions," *Org. Electron.*, vol. 6, no. 3, pp. 129–136, 2005.
- [60] F. Z. Boutebakh, M. L. Zeggar, N. Attaf, and M. S. Aida, "Electrical properties and back contact study of CZTS/ZnS heterojunction," *Optik*, vol. 144, pp. 180–190, Sep. 2017, doi: 10.1016/j.ijleo.2017.06.080.
- [61] Y. Atasoy, M. A. Olgar, and E. Bacaksiz, "Structural, optical and Schottky diode properties of Cu₂ZnSnS₄ thin films grown by two-stage method," *J. Mater. Sci. Mater. Electron.*, vol. 30, pp. 10435–10442, 2019.
- [62] N. Bouguila *et al.*, "Investigation of some physical and photoconductive properties of sprayed CuS₂ film," *J. Mater. Sci. Mater. Electron.*, vol. 33, no. 7, pp. 3810–3821, Mar. 2022, doi: 10.1007/s10854-021-07572-0.
- [63] S. Drissi *et al.*, "Structural, optical and electrical properties of Cu₂CoSnS₄ thin film solar cells prepared by facile sol-gel route," *Thin Solid Films*, vol. 758, p. 139430, 2022.